An Idealized Model Study of the Mass and Heat Transports between the Subpolar and Subtropical Gyres

C. HERBAUT, J. SIRVEN, AND A. CZAJA

Laboratoire d'Océanographie Dynamique et de Climatologie, UMR/CNRS/ORSTOM, Université Pierre et Marie Curie, Paris, France

(Manuscript received 7 February 2000, in final form 6 February 2001)

ABSTRACT

The response of an ocean model of the subtropical and subpolar gyres to idealized surface forcing anomalies that mimic the thermal and mechanical forcing associated with the North Atlantic Oscillation (NAO) is analyzed. Emphasis is given on the subpolar gyre and the mechanisms that drive the mass and heat exchanges between the two gyres. First, steady anomalies are applied. Surface heat flux anomalies induce density gradient anomalies at depth, which drive current anomalies reinforcing the north-eastward mean current separating the two gyres. The northward heat transport of these anomalous currents is 10 times stronger than that associated with the transport of temperature anomalies by the mean current. The heat transport anomalies between the two gyres balances the prescribed surface heat flux after 6–7 yr. A similar mechanism is at work when a decadal harmonic forcing is considered, but the lag is shortened to 3–4 yr. The model response to a wind stress curl anomaly shows a similar behavior to that found with the surface heat flux and primarily enhances the response to the latter. These results suggest that the ocean circulation (both wind driven and thermohaline) is actively involved in the decadal variability, NAO related, of the surface layer at the western subtropical–subpolar gyre boundary.

1. Introduction

The dominant mode of variability of the atmosphere over the North Atlantic is the North Atlantic Oscillation (NAO). The positive phase is associated with a simultaneous strengthening of the Icelandic low and the Azores high, and a strengthening of the polar vortex aloft. The related atmospheric changes at the sea surface are of basin extent, and of considerable amplitude. For instance, the mean sea level pressure difference between Iceland and the Azores is typically 15 mb, and the change associated with NAO extrema is about $\simeq$10 mb (Wallace 1996). Figure 1 shows the surface wind stress and turbulent heat flux anomaly regressed onto the index of the NAO. One sees, in a positive NAO phase, anomalous westerlies centered along 60°N, and anomalous easterlies along 30°N (Fig. 1, top), consistent with the strengthening of the Iceland low and Azores high. These surface wind changes correspond to a modulation and shift of the jetstream and trade winds, associated with a tripolar surface heat flux pattern over the ocean (Fig. 1, middle). The latter is particularly pronounced over the Labrador Sea region, which is a site of deep water formation, and a key region for the dynamics of the Atlantic overturning circulation.

Corresponding author address: Dr. C. Herbaut, Laboratoire D'Océanographie Dynamique et de Climatologie, Université Pierre et Marie Curie, T14 étage 2 CC100, 4 Place Jussieu, Paris Cedex 05 75252, France.
E-mail: ch@lodyc.jussieu.fr

Indices of the NAO show pronounced low frequency fluctuations. The index of Hurrell (1995), displayed in Fig. 1 (bottom), shows a downward trend from the early 1920s to the late 1960s, and a subsequent positive trend, on which are superimposed ''decadal oscillations.'' Various authors (e.g., Kushnir 1994; Marshall et al. 2000) have suggested that the ocean circulation, in particular the North Atlantic circulation, might be involved in these decadal or longer timescales fluctuations.

Many studies have documented the decadal variability of the North Atlantic sea surface temperature (hereafter SST) anomalies (e.g., Deser and Blackmon 1993; Hansen and Bezdek 1996). For the period 1948–92, cold and warm anomalies with lifetime of 3 to 10 yr were identified by Hansen and Bezdek (1996). They seem to move along the mean circulation of the North Atlantic, as also suggested by McCartney et al. (1997) and Sutton and Allen (1997). These decadal SST fluctuations are related to atmospheric anomalies with stronger winds overlying cooler SSTs (Deser and Blackmon 1993).

This variability of the ocean–atmosphere system may arise through the following.

1) *Intrinsic atmosphere variability.* In that case, we can assume that the ocean responds passively to atmospheric forcing.
2) *Intrinsic ocean variability,* with the atmosphere responding passively to oceanic forcing (Delworth et al. 1993, Delworth 1996).

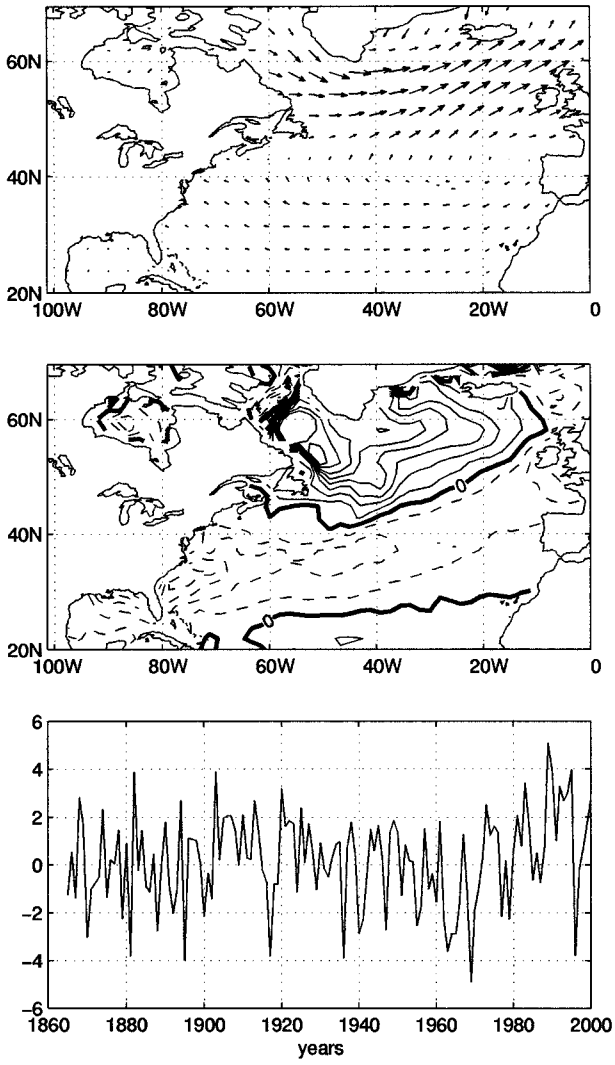

FIG. 1. Observed wind stress (top, arrows with maximum norm of 0.13 N m^{-2}) and surface turbulent heat flux anomaly in W m^{-2} (middle, positive upwards with dashed lines for negative values, CI: 5 W m^{-2}) associated with one standard deviation of the wintertime (Dec–Mar) NAO index of Hurrell (1995) (bottom). The maps are computed by linear regression of wind stress and heat flux anomalies (averaged over Dec–Mar) from the NCAR–NCEP reanalyses onto the NAO index, over the common period 1948–98.

3) *Coupled air–sea interactions* (e.g., Grötzner et al. 1998).

In this paper, we only consider the first hypothesis, and concentrate on the response of the ocean to the surface forcing. However, note that the space and time lags of the ocean response are important for determining how the ocean and atmosphere may be coupled. An atmospheric forcing with a spatial pattern that mimics that of the NAO is defined. The temporal variability is not realistically represented in order to simplify the problem: we restrict the study to a step or harmonic evolution of the idealized NAO. We focus on the evolution of the subpolar gyre, and the mechanisms which drive the mass and heat exchanges between the subtropical and subpolar gyres.

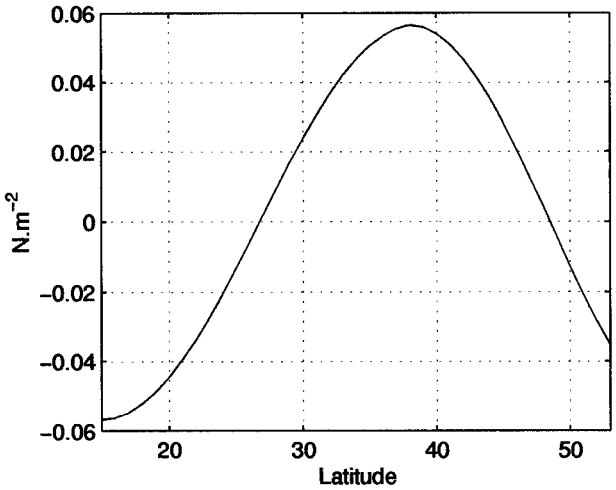

FIG. 2. Mean zonal wind stress W_r used in all the experiments (units: N m^{-2}).

We begin in section 2 with a description of the model, of the numerical experiments, and of the stationnary state simulated by the model in the reference experiment. In section 3, we successively analyze the impact of constant and harmonic surface heat flux anomalies. In section 4, the influence of the wind anomalies is studied. Discussion and conclusions are presented in section 5.

2. The model and the numerical experiments

a. Model setup

We use the Massachusetts Institute of Technology (MIT) primitive equation model (Marshall et al. 1997) limited to an idealized basin of constant depth $H = 4000$ m on a sphere, which extends from 15° to 53°N and

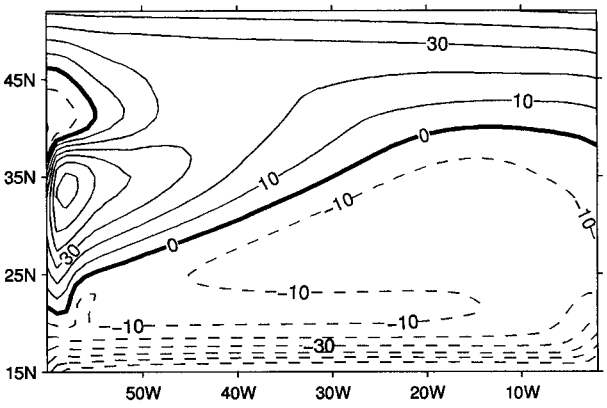

FIG. 3. Diagnosed surface heat flux $-Q_d$ at the final state of REF (in W m^{-2}). Negative values correspond to a heat loss for the atmosphere (CI: 10 W m^{-2}).

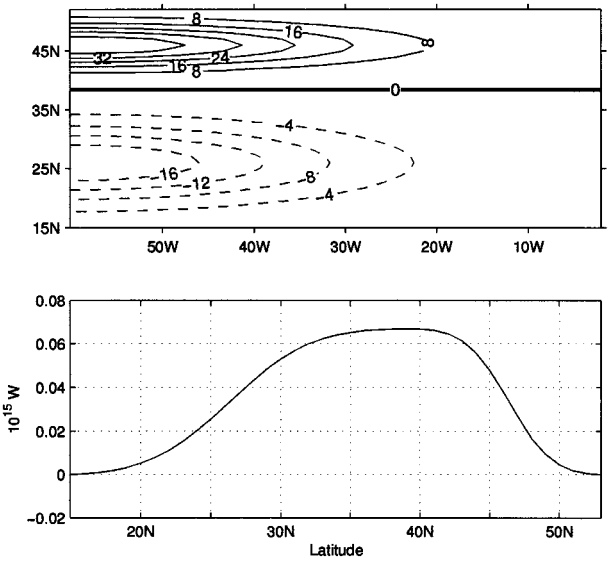

FIG. 4. Surface heat flux anomaly $-Q_a$ in W m^{-2} (top). Oceanic heat transport induced by the heat flux anomaly Q_a in 10^{15} W (bottom).

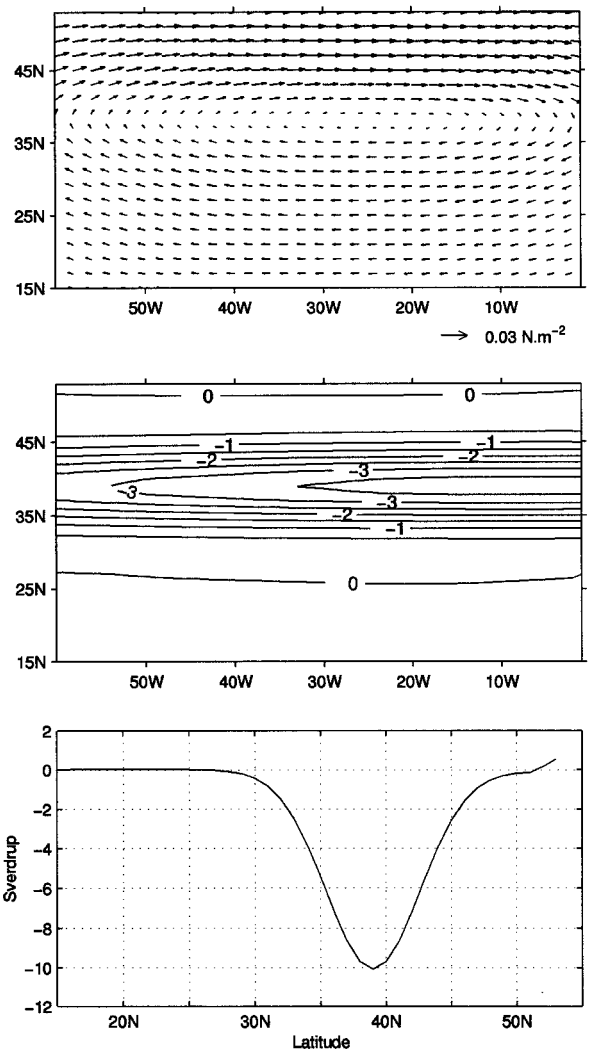

FIG. 5. Wind stress anomaly W_a in N m^{-2} (top), wind stress curl anomaly in 10^{-8} N m^{-3} (middle), and Sverdrup transport induced by the wind stress curl anomaly (bottom).

from 60°W to 0°. The horizontal resolution is 1° × 1°. There are 10 levels on the vertical, with 5 in the upper 600 m. Salinity is not computed by the model so the equation of state of seawater has the simplified form

$$\rho = \rho_0[1 - \epsilon(T - T_0)],$$

where ϵ is a coefficient of thermal expansion ($\epsilon = 2 \times 10^{-4}$ K^{-1}), ρ_0 a mean density ($\rho_0 = 10^3$ kg m^{-3}), and T_0 a reference temperature profile. The horizontal eddy viscosity and thermal diffusivity are, respectively, $K_m^h = 10^4$ m^2 s^{-1} and $K_T^h = 10^3$ m^2 s^{-1}. The vertical viscosity and diffusivity are, respectively, $K_m^v = 10^{-3}$ m^2 s^{-1} and $K_T^v = 10^{-4}$ m^2 s^{-1}. These values are similar to the ones used by Cox (1985) for a similar setup. Convection is parameterized by a nonpenetrative convective adjustment scheme when static instability occurs. No specific formulation is used to parameterize the upper ocean mixed layer processes. A pressure correction method is used to solve the primitive equations and a finite volume approach is employed to discretize the model on a C grid. The temporal scheme is explicit Adams–Bashforth. No-slip boundary conditions are used.

b. The numerical experiments

Six types of numerical experiments are studied in this paper. In the first one, which is the reference experiment, (hereafter noted REF), we use an accelerating convergence method (Bryan 1984) to integrate the model from rest for a period of 480 yr, whereupon a near steady state is achieved. The long-term trends that remain in the deep water are then small. The prescribed surface wind stress W_r used for this integration is zonally constant but varies in latitude (Fig. 2). The zero wind stress curl line that separates the subpolar from the subtropical gyre has been set at 39°N. The surface heat flux Q_r is calculated using the following formula:

$$Q_r = C_0(T_s - T_a), \tag{1}$$

where T_s is the SST, T_a is a zonal atmospheric temperature that varies linearly from 25°C at the southern boundary to 5°C at the northern boundary, and C_0 is a constant, equal to 14.5 W m^{-2} K^{-1}. The heat flux Q_d, diagnosed at the end of the 480-yr period (Fig. 3) has, as expected, a maximum intensity over the northwestern boundary current where it peaks at -60 W m^{-2}.

We have defined heat flux and wind stress anomaly fields (respectively, Q_a and W_a) corresponding to periods of high NAO. The heat flux anomaly Q_a is negative over the subpolar gyre and positive over the subtropical gyre (cf. Fig. 4). The integral over the basin of the

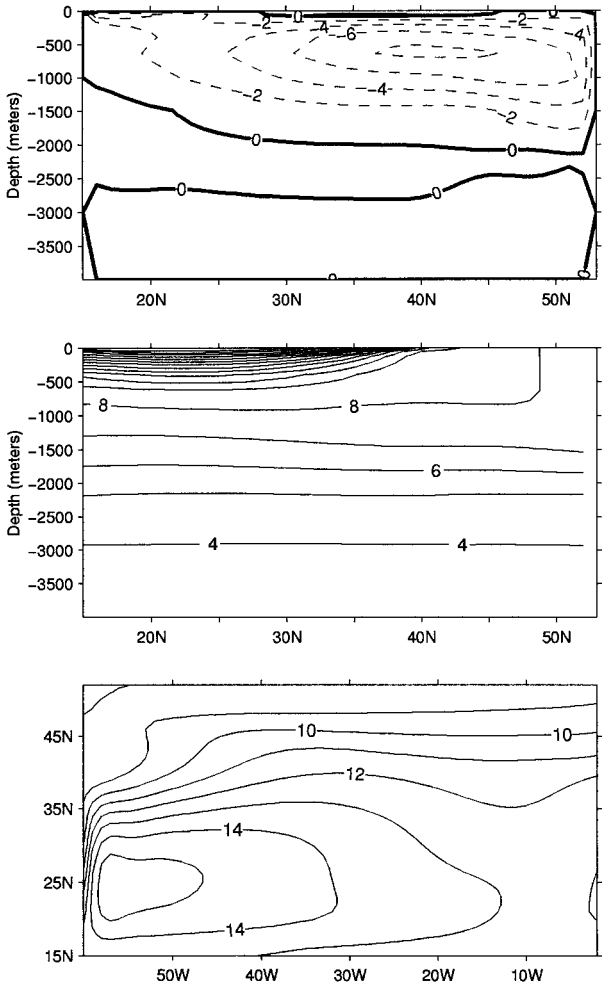

FIG. 6. Meridional streamfunction in Sv (top), north–south section of temperature at 58°W (middle), and temperature at 300 m (bottom) in experiment REF.

prescribed anomaly is null. The wind stress anomaly, W_a is elliptic, centered at 39°N where the curl of the wind stress W_r is null (cf. Fig. 5). These anomaly fields were used to perform ten numerical experiments.

Two types of runs initialized with the final state of the 480-yr period are integrated for 18 yr with constant forcing fields. In the first one, the atmospheric heat flux is the sum (experiment CQ_+) or the difference (experiment CQ_-) of the diagnosed heat flux Q_d and a constant anomaly Q_a (Fig. 4, top). The anomalous heat transport of the ocean required to balance the thermal forcing anomaly at equilibrium is found to be northward, peaking near 39°N, with a maximum amplitude of about 0.06 $\times 10^{15}$ W (Fig. 4, bottom). As shown in Marshall et al. (2000), a similar amplitude is found when the observed NAO surface heat flux anomalies are used to compute the oceanic heat transport. The wind stress is the same as in REF: W_r. In the second one, the heat flux is Q_d but a wind stress anomaly W_a (Fig. 5) is added (experiment CW_+) or substracted (experiment CW_-) to the wind stress W_r used in REF. Experiment CW_+ (CW_-) reproduces the strengthening (weakening) and the northward (southward) shift of the westerlies seen in a positive (negative) NAO phase. Unlike W_r, W_a is zonally varying, and its meridional extent is that of the basin. Application of linear (flat bottom) Sverdrup balance indicates that W_a drives an anticyclonic circulation [the intergyre gyre of Marshall et al. (2000)], with a maximum barotropic mass transport of 10 Sv (1 Sv = 10^6 $m^3\ s^{-1}$) at equilibrium. The maximum is reached on the line where the Ekman pumping vanishes (Fig. 5, bottom), hereafter called the $w_e = 0$ line. A similar mass transport is obtained when applying the Sverdrup relation to the observed NAO wind stress curl (not shown). These experiments with constant forcing are mainly devoted to the study of the transient phenomena and the determination of timescales associated with the system.

Spectral analysis of the observed NAO index indicates enhanced power near the decadal band (Hurrell and Van Loon 1997), which has been interpreted as a possible indication of coupling between the atmosphere and the ocean circulation in the North Atlantic on this timescale (Grötzner et al. 1998; Marshall et al. 2000). To gain some insight into the dynamics of the wind driven and the meridional overturning circulation at decadal timescales, we have conducted experiments with idealized harmonic forcings. In nature, there is a strong temporal correlation between the patterns of NAO surface heat flux and wind stress shown in Fig. 1. Here, we will first analyse experiments in which only the heat flux (VQ) or the wind stress (VW) are allowed to vary with a simple sinusoidal dependance, eventually analyzing the combined thermal and mechanical forcing (VQW). To illustrate the decadal behavior, we will consider harmonic forcing at 10 (experiments VQ_{10}, VW_{10}, and VQW_{10}) and 20 (experiments VQ_{20}, VW_{20}, and VQW_{20}) yr. These experiments are summarized in Table 1.

c. The modeled circulation in REF

Figure 6 summarizes the state of the ocean at the end of year 480 in experiment REF. The model reproduces the essential characteristics of the circulation in the North Atlantic. There is a pronounced thermocline south of 40°N, penetrating to about 500 m (Fig. 6, middle), associated with a subtropical gyre that is weaker than observed (the barotropic transport along the western boundary is only 21 Sv). The meridional overturning, which peaks at 8.5 Sv (also too weak), consists in a sinking branch at high latitudes and upwelling in the subtropics (Fig. 6, top). The subpolar gyre has a small horizontal extension, as can be inferred from the small departures from zonality in the temperature field at 300 m (Fig. 6, bottom). It is the site of intense convection, particularly in the northwestern corner, where convection can reach 800 to 1000 m, and where the coldest waters are found. The whole circulation is similar to

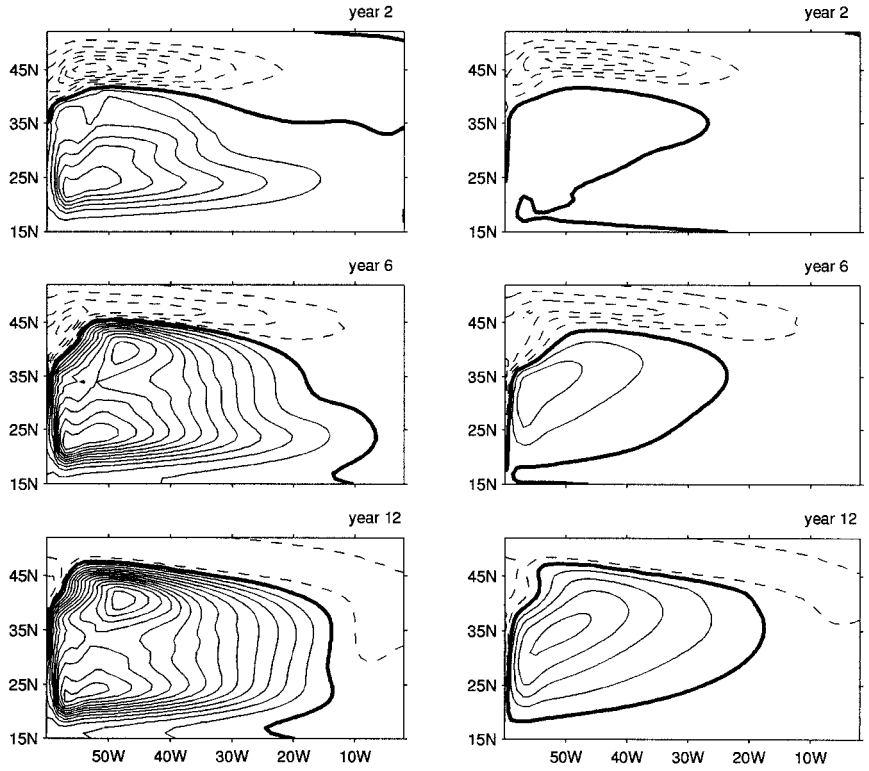

FIG. 7. Differences of temperature between experiment CQ_+ and experiment REF, at years 2, 6, and 12, in surface (left) and at 300 m (right). Solid lines indicate positive values and dashed lines negative values (CI: 0.2°C).

that obtained by Cox (1985) and Colin de Verdière (1989).

The region that separates the subtropical and subpolar gyres is of special interest. The current that separates them [hereafter CSG (current separating the two gyres)] is tilted slightly northward. The mass and heat exchanges between the gyres across the $w_e = 0$ line are mainly confined between 60° and 40°W. In the upper 800 m, they reach respectively 8 Sv and 8×10^{15}W and are balanced by a southward transport along the western boundary in the deeper layer. The upper layer mass transport is associated with a meridional heat transport equal to 0.4×10^{15}W across the $w_e = 0$ line.

These results are close to those of Holland (1977) who has spun up an ocean model in a similar setup with a constant wind stress similar to W_r. However, we note two important differences:

- The two gyre circulation obtained in Holland (1977) includes a much larger subpolar gyre. Indeed, adding the heat flux forcing reduces the horizontal extension of the subpolar gyre compared to the purely wind driven case.
- In Holland's experiment, along the latitude where the Ekman pumping vanishes, the meridional velocity cancels, the current is eastward, and there is neither instability nor exchange between the gyres; Holland links these results to the strong dissipation and the low resolution he uses. Adding the heat flux forcing obviously creates strong exchanges of mass and heat between the two gyres.

3. Impact of an atmospheric heat flux anomaly

In this section, we investigate the ocean response to a surface heat flux anomaly, which mimics period of high (experiment CQ_+) or low (experiment CQ_-) NAO. As mentionned in section 2b, the oceanic heat transport required to balance the steady forcing is northward (southward) in positive (negative) NAO phase, with a maximum of about 0.07×10^{15}W (Fig. 4). This gives an estimate of the heat transport changes expected in the simulations. We will focus on determining which mechanism (waves or advection) controls the ocean adjustment toward a steady state in $CQ_\pm$, and study its sensitivity to a time-dependent forcing in $VQ_{10,20}$.

a. Impact of constant atmospheric heat flux anomalies

1) EXPERIMENT CQ_+

In the subtropical gyre (see Fig. 7), the surface water quickly warms up until year 12 when a near stationnary state is reached. At that time, the SST has increased by

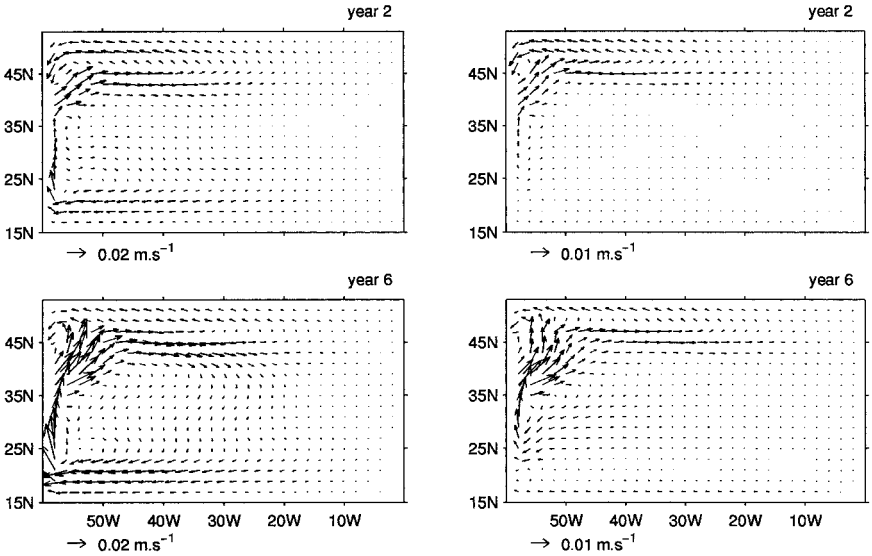

FIG. 8. Current anomalies, at years 2 and 6, in experiment CQ_+ in surface (left) and at 300 m (right).

3.6°C near 50°W in the western part of the basin. Below 200 m, a positive anomaly pattern also develops: in the first 4 yr, the warming remains weaker than 0.2°C, and after 12 yr it reaches a steady state with a maximum anomaly of 0.8°C. The meridional heat transport at any latitude along the western boundary varies in phase with the meridional heat transport across the $w_e = 0$ line (not shown), which could be attributed to the propagation of Kelvin waves along the basin boundaries. Although fast propagating Kelvin waves play a role in the oceanic adjustment to this heat flux forcing, they do not set its timescale, which is determined by other oceanic processes (see below).

In the subpolar basin, during the first 2 yr, the dominant process that drive the temperature response to the surface heat flux is the vertical mixing due to convective adjustment. The shape of the negative SST anomaly mimics the heat flux pattern, except along the western boundary where the minimum is shifted southward of the heat flux, because of advection by the boundary current. Where the stratification is weak (i.e., north of 45°N and in the western part of the subpolar gyre), the cooling by convection reaches 600 m. It reinforces the mean temperature gradient at the $w_e = 0$ latitude, with a maximum located between 55° and 50°W, and therefore enhances the mean northeastward current (Fig. 8,

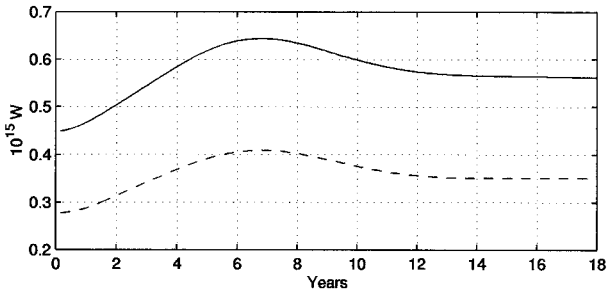

FIG. 9. Time evolution of the heat transport across the $w_e = 0$ line in the upper 600 m (solid line) and in the upper 200 m (dashed line) in experiment CQ_+.

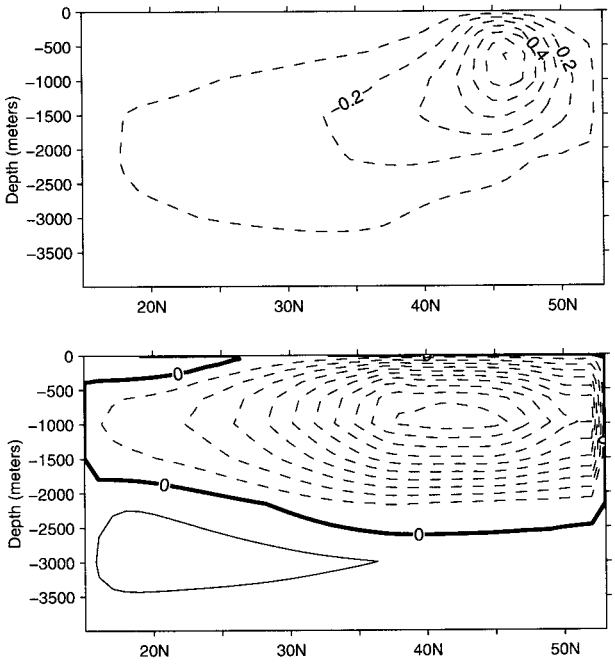

FIG. 10. Differences between the meridional streamfunction in experiment CQ_+ and the meridional streamfunction at the end of experiment REF after 6 months (top; CI: 0.2 Sv) and after 7 yr (bottom; CI: 0.4 Sv).

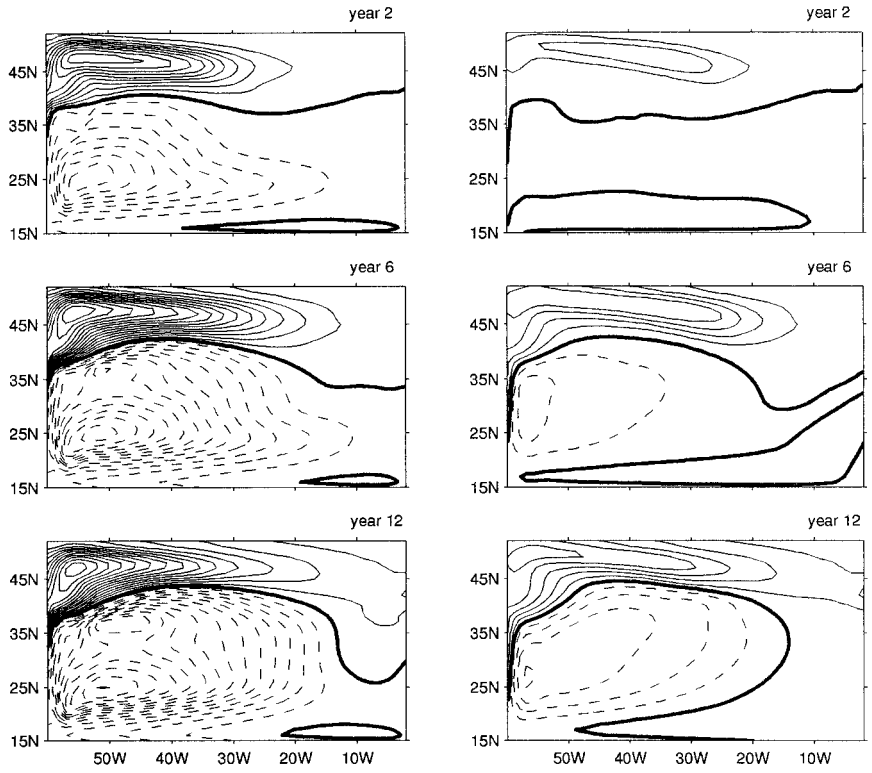

FIG. 11. Differences of temperature between experiment CQ_ and experiment REF, at years 2, 6, and 12, in surface (left) and at 300 m (right). Solid lines indicate positive values and dashed lines negative values (CI: 0.2°C).

top). After 3 yr, the northward heat transport in the upper 200 m across the $w_e = 0$ line starts to dominate the evolution of the integrated heat budget in the subpolar basin. At first, heat is transported eastward by the stronger CSG and warms the southeastern part of the subpolar basin, while it is unable to compensate the heat losses in the western part, which goes on cooling. Consequently, the east–west temperature gradient and the heat transport at $w_e = 0$ keep on increasing. This heat transport increase is associated with an increasing northward tilt of the current anomaly. After 6–7 yr, the anomalous current has tilted northward (Fig. 8, bottom) and advects warm water toward the western and northern parts of the subpolar gyre. Anomalous northward heat transport in the upper 600 m dominates over the surface heat losses everywhere in the subpolar basin. The system enters a new phase with slightly increasing temperature in the western part, reducing the east–west temperature gradient and the northward heat transport. The time evolution of cross gyre heat transport (Fig. 9) is thus nonmonotonic with a maximum increase of 0.2×10^{15} W in the upper 600 m, larger than the required equilibrium value of 0.07×10^{15} W (cf. Fig. 4). After 12 yr, the SST has increased in the subpolar basin south of 45°N, except between 60° and 55°W where the strongest cooling has appeared (it peaks at −1°C). North of 45°N, the cooling is about 0.3°C (Fig. 7). Afterward the variations of the system become very small.

As there is no anomalous input of momentum in this experiment, the increase of the northward transport is compensated by a southward transport below 1000 m. Consequently, the adjustment described above is associated with an intensification of the meridional overturning (Fig. 10). The maximum of the streamfunction anomaly (defined as the difference between the overturning streamfunction at time t and the overturning streamfunction diagnosed at the end of REF) is confined in the northern part of the subpolar basin during the first year. It then grows and moves slowly to its southern part. Indeed, as the stratification is initially stronger in the south of the subpolar basin, deep convection occurs there with some delay. After 7 yr, the convection anomaly is reduced in the subpolar basin and the meridional overturning anomaly starts to decrease, reaching a near steady state after 12 yr.

To sum up, the weakly stratified waters located in the north western part of the subpolar gyre allow an easy penetration of the surface heat flux anomalies down to 800 m, which build anomalous density gradients in the thermocline. The latter drive in turn large anomalous currents, which govern the ultimate evolution of SST ($V'T_0 \gg V_0T'$) close to the $w_e = 0$ line. A more quan-

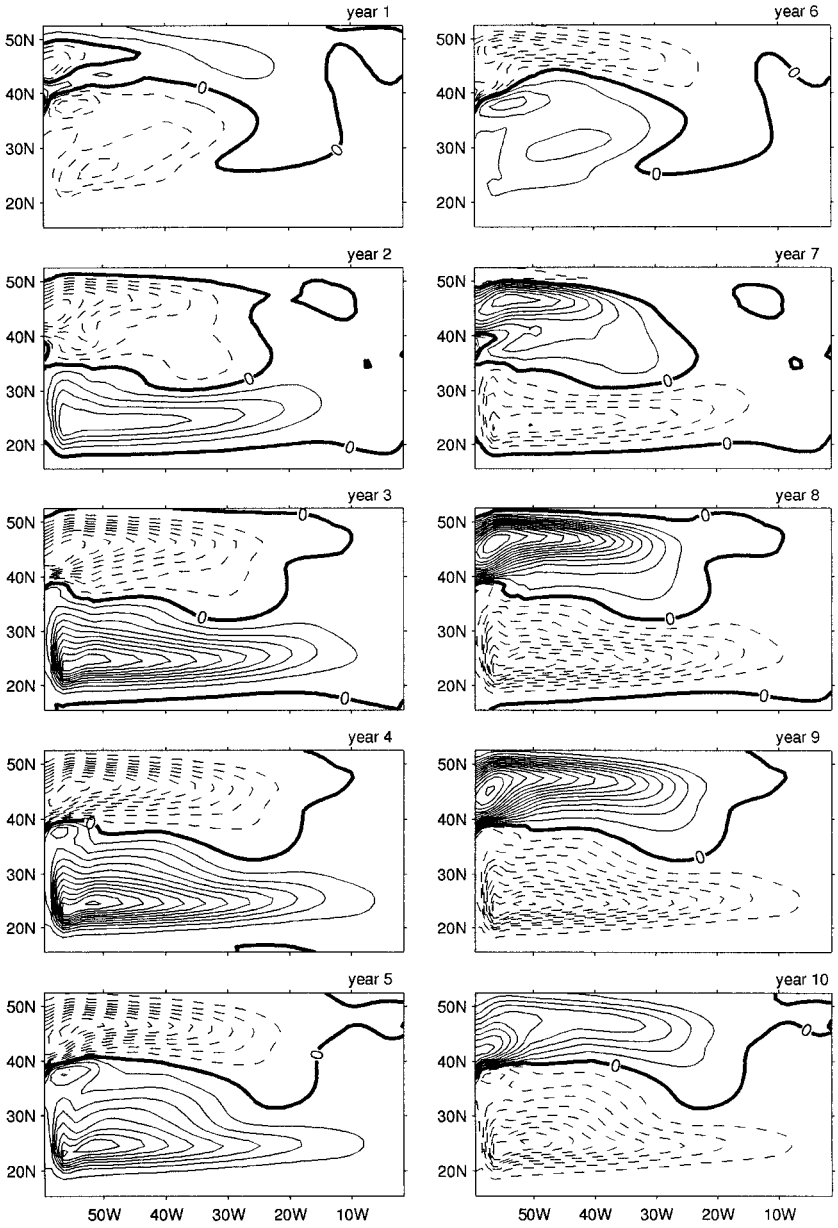

FIG. 12. SST anomalies over the last decade of integration in experiment VQ_{10}. Solid lines indicate positive values and dashed lines negative values (CI: 0.2°C).

titative and detailed analysis of the surface heat budget is presented in the next section.

2) EXPERIMENT CQ_-

A similar experiment performed with a heat flux anomaly corresponding to a low NAO shows that the response is not simply the reverse of that observed in CQ_+ (Fig. 11). The main differences are found in the subpolar gyre, where strong SST anomalies are maintained after 6 yr (cf. Fig. 7 with Fig. 11). This illustrates that the heat transport across the $w_e = 0$ line is not dominated by V_0T', since, in that case, the SST anomaly generated in the subtropical gyre would have been advected into the subpolar gyre. The variations of the heat transport in the upper layer have a similar amplitude as that obtained in experiment CQ_+ but an opposite sign. However, the adjustment timescale is longer (10 yr instead of 7 yr, not shown). The response is not antisymmetric because the vertical stratification differs in the subpolar and subtropical gyres. As a consequence, the negative temperature anomaly observed during the pos-

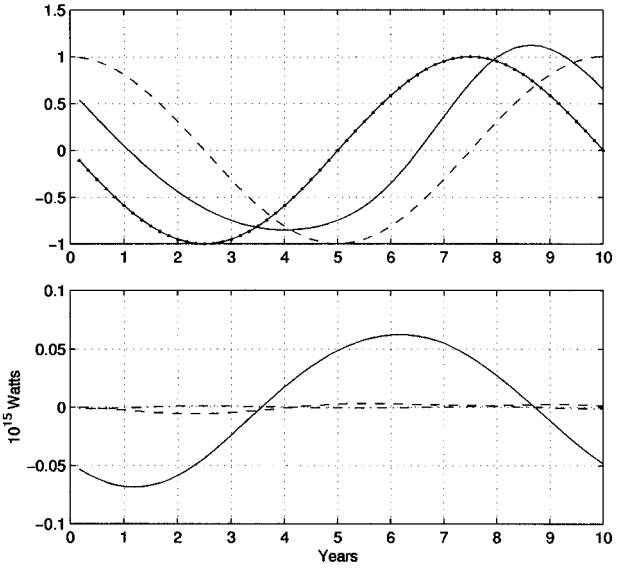

FIG. 13. (top) Evolution of the upper 50-m temperature averaged over the area 60°–30°W, 39°–53°N (solid line) over the last 10 yr of experiment VQ_{10}. The variations of the mean temperature over the same area due to the atmospheric heat flux anomaly are indicated by a dashed line. This curve has been normalized by its maximum (i.e., 4°C). The atmospheric heat flux anomaly, normalized by its maximum, is also displayed (dot–dashed line). (bottom) Contributions to the upper 600-m heat transport across the $w_e = 0$ line in experiment VQ_{10} (in 10^{15} W). Solid line indicates $V'T_0$, dashed line V_0T and dot–dashed line $V'T'$.

itive NAO phase in the subpolar gyre extends deeper than the negative temperature observed during the negative NAO phase in the subtropical gyre.

b. *Impact of a variable atmospheric heat flux anomaly*

1) EXPERIMENT VQ_{10}

The model response to a 10-yr harmonic forcing is found to be a perfect 10-yr oscillation, so that we only analyze the last 10 yr of the 100-yr integration. Temperature anomalies are computed by substracting the mean over the last 10 yr. The surface forcing is zero at $t = 0$ and 10 yr, with maximum heat loss (maximum heat gain) over the subpolar gyre at 2.5 yr (7.5 yr).

During the first 5 yr of the cycle, the circulation adjusts as described in CQ_+ with some differences on the time scale due to a weaker amplitude of the forcing. During the first two years, enhanced deep convection is confined in the northern part of the subpolar basin. It takes 3 yr before the anomalous heat flux erodes the upper stratification in the southwestern part of the subpolar basin, and the density anomalies extend to deep layers (around 800 m at 40°N, 55°W). After 4 yr, the temperature anomaly over the subpolar basin reaches a minimum and the SST anomaly pattern looks like that observed after two years in CQ_+ (Fig. 12). Then, as in CQ_+, the positive SST anomaly extends in the subpolar gyre. After 5 yr, the heat flux anomaly changes sign. Restratification quickly occurs in the subpolar gyre, and the positive SST anomaly previously created is reinforced. The maximum of the SST anomaly is reached between 8 and 9 yr with a pattern looking like that obtained in CQ_- after 2 yr.

A synthetic description of the time evolution of the temperature is given in Fig. 13, which shows the upper 50-m mean temperature (solid line) computed over the western part of the subpolar basin. The variations of the mean temperature in the upper layer due to the atmospheric heat flux are also displayed in dashed line (this curve is obtained by integrating the equation $\rho C_p h \partial_t T = Q$). The difference between the amplitude of the curves which reaches 3°C illustrates the strong impact of the advection (during the period of negative atmospheric heat fluxes, entrainment brings heat into the upper layer and also contributes to this difference). Lags of 1 yr during the cold period, and of 1.5 yr during the warm period are also noticeable. These lags reflect the variations of heat transport between the basins. The total heat transport in the upper 600 m (which is northward) is minimum after about 1 yr and maximum after 6 yr (Fig. 13, bottom). The variations of the heat transport are well explained by the advection of the mean temperature by the fluctuations of the meridional current ($V'T_0$ term). The amplitude of the variations of the heat transport at 39°N in the upper 600 m is reduced by a factor 2 with respect to the variations obtained after adjustment in experiments $CQ_\pm$.

The meridional overturning displays variations of ± 2 Sv. In the first 2 yr, northern enhanced convection increases locally the strength of the overturning. As deep convection extends to the southwestern corner of the subpolar basin, the maximum of the overturning moves southward. When the surface heat flux forcing switches from cooling to warming, the convection is reduced, but the overturning does not respond instantaneously: its maximum is reached after 6 yr. The increase of the transport between the gyres, after 5 yr, feeds the overturning and induces a lag of $6 - 2.5 = 3.5$ yr between the maxima of the heat flux anomaly and of the overturning.

2) EXPERIMENT VQ_{20}

The evolution of the SST anomalies is similar to that obtained in experiment VQ_{10}. The SST anomaly patterns oscillate between those which characterized CQ_+ and CQ_-. As the negative phase of the atmospheric heat flux anomaly lasts longer than in VQ_{10}, the minimum of the SST anomaly over the subpolar gyre is 1°C lower than in VQ_{10}. Similarly, the upper 600-m heat transport across the $w_e = 0$ line has an amplitude twice higher than in experiment VQ_{10}, but it still lags the forcing by about 4 yr.

In conclusion, the mechanisms evidenced in $CQ_\pm$ are still found when considering a low frequency time-de-

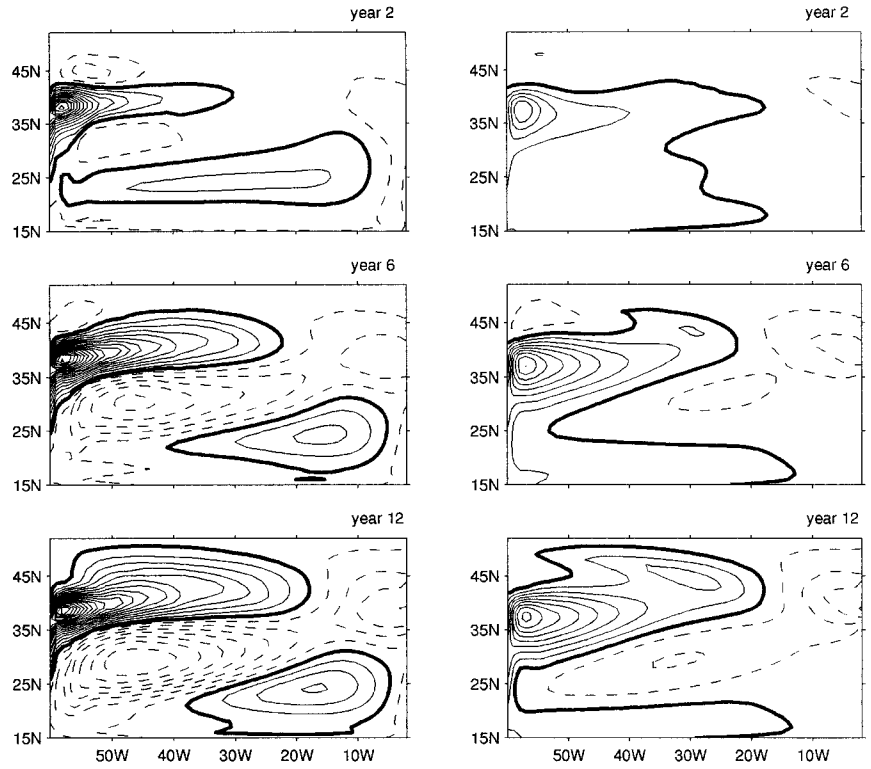

FIG. 14. Differences of temperature between experiment CW_+ and experiment REF, at years 2, 6, and 12, in surface (left) and at 300 m (right). Solid lines are for positive values and dashed lines for negative values (CI: 0.2°C).

pendent forcing. Advection dominates, and the variations of the heat transport are driven by anomalous currents acting on mean SST gradients. The temporal lag between the forcing and the ocean response is 3–4 yr when the forcing is time varying, independantly of its period (10 or 20 yr). It is much longer when the forcing is steady. The ocean response to a surface heat flux forcing is non linear, with a more vigorous and faster response in positive than in negative NAO phase.

4. Impact of the wind

a. Effect of a constant wind anomaly

1) EXPERIMENT CW_+

Figure 14 shows the temperature anomalies at the surface and at 300 m after 2, 6, and 12 years of integration. At both depths, a positive anomaly develops along the $w_e = 0$ line, then extends northward into the subpolar gyre. The development of this anomaly is the result of three different mechanisms. First, the wind stress anomaly induces an instantaneous barotropic response, evidenced for example on the barotropic streamfunction (not shown), which reinforces the western boundary current between 34° and 42°N. As there is a strong temperature gradient between these two latitudes along the western boundary, the difference between the northward heat transports at 34° and 42°N increases, even if the difference between the mass transports does not change. This convergence of heat transport generates a positive temperature anomaly, which is located along the western boundary, and which is then advected into the interior of the basin by the mean current. This response remains localized between 60° and 45°W within the first years of integration. Second, as shown by Fig. 15, the deepening of the 8°C isotherm along the $w_e = 0$ line in the area limited by 50° and 20°W, which is due to a local response to the negative Ekman pumping anomaly, is partially stopped after the passage of a long baroclinic Rossby wave front. The velocity estimated from Fig. 15 is equal to 2 cm s^{-1}. It agrees with the phase velocity of the first baroclinic mode computed from the stratification observed in the model at 39°N, using the classical linear theory. Thus, the first baroclinic mode long Rossby wave, which propagates westward without being affected by the mean flow in agreement with theory (non-Doppler shift effect: see Liu 1999 and Sirven and Frankignoul 2000) partly explains the behavior of the model (around the $w_e = 0$ line). Third, after 12 yr, the influence of advection by the mean current is no longer concentrated in the western part of the basin, and the anomaly is advected northward in the subpolar gyre.

In this experiment, the divergence of the horizontal heat transport due to the advection of SST by the Ekman

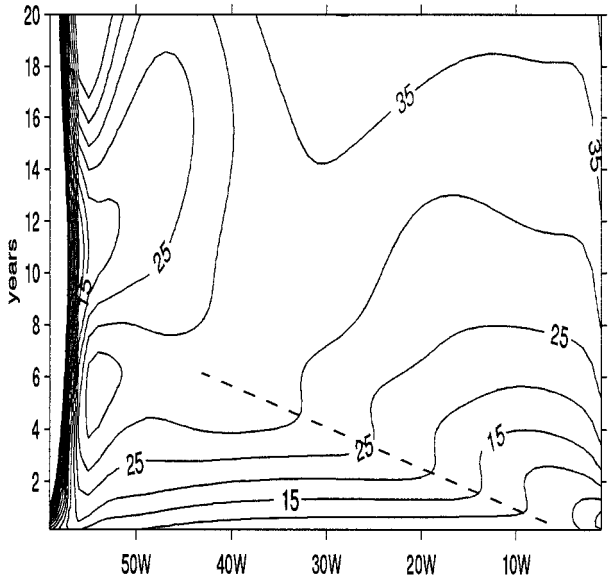

FIG. 15. Evolution of the differences of the 8°C isotherm depth at 39°N between experiment CW_+ and experiment REF (in m). The wave front positions are indicated by a dashed line.

current has a significant impact only in the western part of the subpolar gyre (cooling near 45°N, in the first years) and in the southern part of the subtropical gyre (warming near 25°N–20°W, during the first years). The pseudo air–sea Ekman heat flux associated with a positive phase of NAO reaches a maximum heat loss of 16 W m^{-2} over the subpolar gyre as displayed by Fig. 2.4 of Marshall et al. (2000), while in CW_+ the maximum heat loss is only 4 W m^{-2}. This difference might be due to the poor representation of the climatological SST in the model.

The variations of the heat transport are weaker in experiment CW_+ than in experiment CQ_+. During the first 6 months, the total heat transport in the upper 600 m across the $w_e = 0$ line decreases by around 10%. Afterward, it increases by 0.07×10^{15} W to reach a maximum after 7–8 yr (which corresponds to the time it takes for a first baroclinic Rossby wave to propagate across the basin at 39°N).

The time evolution in the subtropical gyre, south of 35°N (ventilated area) has been studied in great details by Ezer (1999), with a more realistic model than that used here. So we will not develop this point. We only

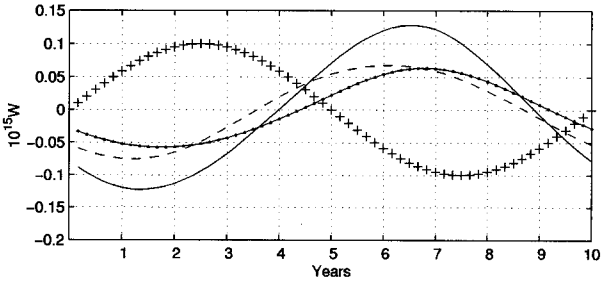

FIG. 16. Upper 600-m heat transport across the $w_e = 0$ line in the experiments VWQ_{10} (solid line), VQ_{10} (dashed line), and VW_{10} (dot–dashed line) in 10^{15} W. The mean values have been substracted and are respectively equal to 0.443, 0.451, 0.442×10^{15} W. The forcing (the model NAO index), normalized to 0.1, has been superimposed (crosses).

emphasize that, in agreement with Ezer (1999), the variations of the western boundary current mainly depend on propagation of the first baroclinic mode Rossby waves (see also Sturges and Hong 1995 and Sturges et al. 1998) while the core of the subtropical gyre is also affected by the second baroclinic mode Rossby waves as suggested by Liu (1999) or Sirven and Frankignoul (2000).

2) EXPERIMENT CW_-

Contrary to CQ_- which is not the reverse of CQ_+ because of convection, experiment CW_- shows a response that is the opposite of that observed in CW_+. There are the same anomaly patterns with an opposite sign, and a similar but opposite behavior for the heat transport at 39°N. This result suggests a stronger linearity of the response to wind stress forcing and is in agreement with the important role played by Rossby waves, which are linear to a good approximation.

b. Impact of a variable wind anomaly

1) EXPERIMENT VW_{10}

As for experiments VQ_{10} and for the same reasons, only the last 10 yr are analyzed. The prescribed surface forcing evolution is shown in Fig. 16 (crosses). Temperature anomalies are computed by substracting the mean over the last 10 yr. Anomalies at years 4 and 9, respectively, look like the anomalies after 2–3 yr in

TABLE 1. The experiments whose acronyms begin with a C are made with constant forcing. Those whose acronyms begin with a V are made with a variable forcing. The periods in VQ, VW, and VQW are equal to 10 or 20 yr as indicated by the indices.

Experiment	Heat flux	Wind	Initial state	Length (yr)
REF	$Q_r = C_0(T_s - T_a)$	W_r (constant)	Rest	480
$CQ_\pm$	$Q_d \pm Q_q$	W_r	Year 480 of REF	18
$CW_\pm$	Q_d	$W_r \pm W_a$	Year 480 of REF	18
$VQ_{10,20}$	$Q_d + Q_a \sin wt$	W_r	Year 480 of REF	100
$VW_{10,20}$	Q_d	$W_r + W_a \sin wt$	Year 480 of REF	100
$VQW_{10,20}$	$Q_d + Q_a \sin wt$	$W_r + W_a \sin wt$	Year 480 of REF	100

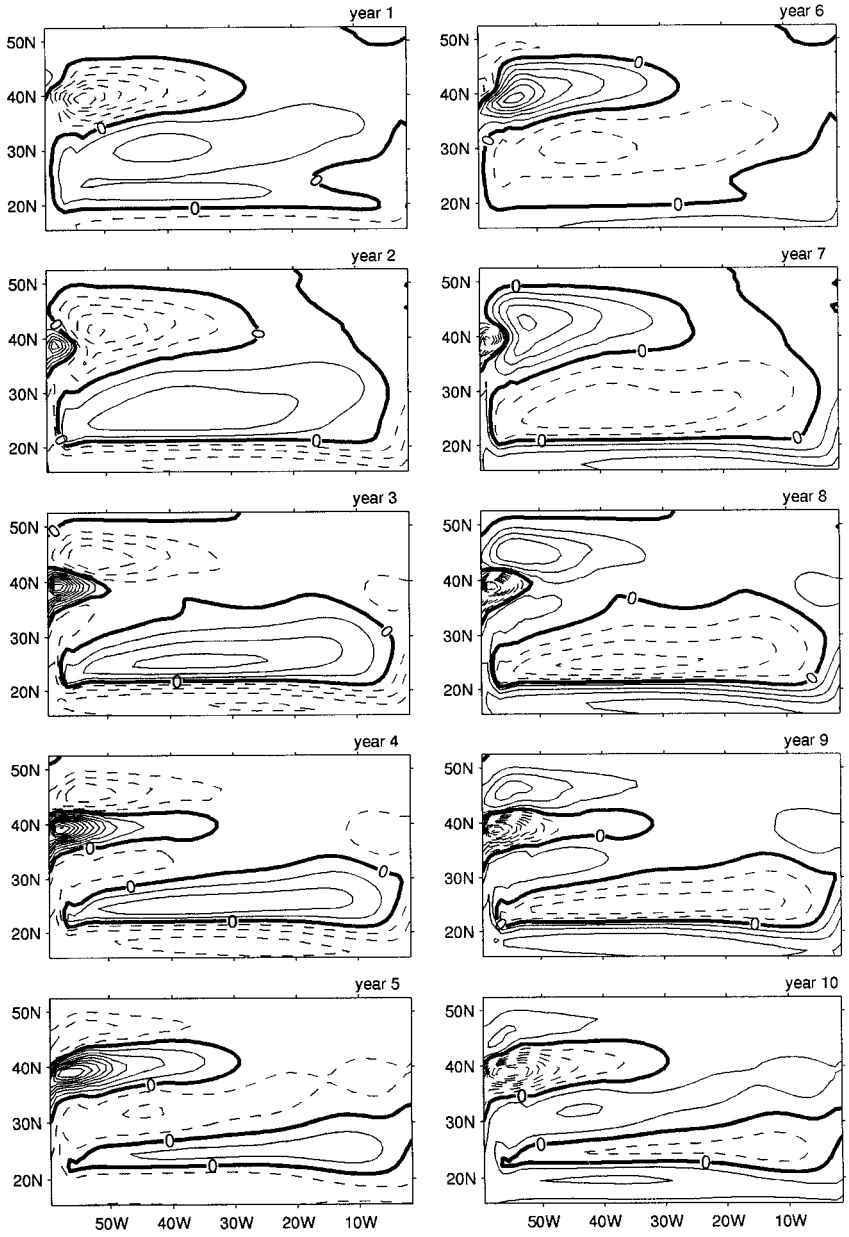

FIG. 17. SST anomalies over the last decade of integration in experiment VW_{10}. Solid lines indicate positive values and dashed lines negative values (CI: 0.2°C).

experiment CW_+ and CW_- (Fig. 17). The model oscillates between these two states. The heat transport at 39°N in the upper 600 m displays a harmonic behavior with an amplitude equal to 0.06×10^{15} W (Fig. 16). It follows by about 4 yr the atmospheric forcing. Heat transport variations in VQ_{10} and VW_{10} are very similar (Fig. 16, dashed and dot–dashed curve, respectively). However, the advection of the temperature anomalies by the mean current is not negligible in VW_{10} because the temperature anomaly generated at the western boundary is partly advected by the mean current, as in experiment CW_+. Advection of temperature anomalies by the mean current is typically 30% of that due to anomalous current acting on mean temperature gradients.

The meridional overturning shows also substantial variations. It oscillates from 7.4 to 9.8 Sv. Part of these variations are explained by the strong Ekman transport at the northern boundary. Indeed, along the northern boundary, the mixed layer is deep (around 800–1000 m), therefore the upwelling (downwelling) compensating the southward (northward) Ekman transport reaches

deep layers and generates an anomaly of the meridional streamfunction which extends to 1000 m. The variations of the heat transport and the meridional overturning have amplitudes comparable to those obtained in VQ_{10}.

2) EXPERIMENT VW_{20}

The SST anomalies show a similar evolution as in experiment VW_{10}, with more extended patterns and higher extrema. The amplitude of the variations of the heat transport in the upper 600 m across the $w_e = 0$ line is very close to that observed in VW_{10}. The delay with respect to the atmospheric forcing is slightly longer (4–5 yr).

c. Impact of variable wind and heat flux anomalies

Experiments with both harmonic atmospheric heat flux and wind anomalies were performed ($VQW_{10,20}$). The temperature anomalies obtained over the last 10 yr of integration in VQW_{10} have similar patterns as those obtained by summing the temperature anomalies obtained in VW_{10} and VQ_{10}. The variations of the heat transport in the upper 600 m across the $w_e = 0$ line are also quasi equal to the sum of the variations computed in VQ_{10} and VW_{10} (Fig. 16). Similar results are obtained with VQW_{20}. Hence, as in Ezer (1999), the ocean responds linearly to the combined effect of wind and heat flux anomalies.

5. Discussion and conclusions

This study has investigated some aspects of the response of a simple ocean general circulation model (the MIT model of Marshall et al. 1997) limited to the subtropical and subpolar gyres, to different idealized surface forcing anomalies mimicking the spatial pattern of the NAO. Our approach, which consists in imposing fixed heat fluxes and wind stress anomalies in separate experiments, enables a simple interpretation of the results. These experiments highlight the basic mechanisms potentially at play in the decadal variability of the North Atlantic.

Our experiments show a significant role of geostrophic currents in modulating the low frequency behavior of SST anomalies at the western subtropical–subpolar gyre boundary. This is in good agreement with the numerical study of Halliwell (1998), who analyzes the surface heat budget of a more realistic OGCM forced by observed atmospheric circulation anomalies and finds that advective effects are primarily governed by the anomalous currents acting on the SST gradients. In all simulations (thermal and mechanical forcings), we find that the oceanic adjustment to the atmospheric forcing is mainly controlled by heat exchanges between the subpolar and subtropical gyres. In response to a constant heat flux characteristic of a positive NAO phase, the northward heat transport between the gyres increases. This heat transport results from the building of density gradients at depth in the subpolar gyre, which generate a northward advection of the mean temperature by the current anomalies (term $V'T_0$). However, in the experiments where a wind stress anomaly is imposed, the role of the advection of the temperature anomalies by the mean current (term V_0T') is no longer negligible since it provides 30% of the total heat transport in the upper 600 m across the $w_e = 0$ line. How our results may relate to the observations of Hansen and Bezdek (1996) or Sutton and Allen (1997)—who show propagation of SST anomalies along the North Atlantic Current and thus emphasize the role of the term V_0T'—is nevertheless difficult to assess, owing to the idealized mean circulation produced by the model. Moreover, it is difficult to estimate the relative importance of the terms V_0T' and $V'T_0$ from observations.

The overturning circulation is found to adjust rather quickly to the thermal forcing associated with the NAO. The temporal lag between the thermal forcing and the oceanic heat transport across the subtropical–subpolar gyres boundary is about 3–4 yr when a prescribed harmonic forcing is used, at both 10- and 20-yr period. Eden and Willebrandt (2001) find at a 12-yr period a damped oscillation of the dynamic height anomaly in a principal oscillation pattern analysis of a more realistic simulation of the Atlantic Ocean, forced by observed surface heat flux anomalies only. They find a time lag between the surface forcing in the Labrador sea (directly related to the NAO) and the strength of the overturning circulation in the North Atlantic of 2–3 yr in good agreement with our experiments with harmonic forcing. A similar temporal lag is also found by Häkkinen (1999).

The adjustment timescale in the experiments with harmonic heat flux anomaly is similar to that associated with the wind driven circulation and suggests that the thermohaline and wind driven circulations compete with one another in determining the full ocean response to the NAO forcing. We find that this interaction is essentially linear and constructive (the total response is stronger than either that obtained solely with thermal or mechanical forcing), with similar amplitudes and phases for mechanical and thermal responses. This is in agreement with Ezer (1999).

Our simulations certainly overestimate the impact of the heat flux forcing compared to that of the wind. The strong current anomalies between the subpolar and subtropical gyres observed in our experiments are induced by a strong deepening or shoaling of the mixed layer north of the intergyre boundary. In the real North Atlantic, the mixed layer north of the Gulf Stream and of the North Atlantic Current is, however, shallow because surface salinity is weak (Levitus 1986), so the building of strong density gradients seen in the thermally forced experiments may be less efficient in nature. Also, the east–west temperature gradient along the intergyre boundary is weaker in the model than in the observations. This could underestimate the heat transport of the

intergyre–gyre circulation suggested by Marshall et al. (2000), and consequently the role of the wind stress. In addition, we note that, as suggested by the recent experiments of Eden and Willebrandt (2001), the inclusion of topography may modify the Sverdrup-like solutions that we have obtained in the surface wind forced experiments.

Finally, the mechanism described in experiment $CQ_{\pm}$ and $VQ_{10,20}$ could participate to the decadal oscillation of the thermohaline circulation observed in a forced climate model (Hakkinen 2000). The experiments with wind show an important heat transfert between the gyres that could be part of the coupled mechanism suggested by Grötzner et al. (1998) to explain the decadal variability observed in their coupled climate model.

Acknowledgments. We thank G. de Coëtlogon, C. Frankignoul, and G. Reverdin for many fruitful discussions, and for comments on an earlier version of this manuscript. Comments by two anonymous reviewers were most helpful to improve the manuscript. Support from the European community (EC Grant EVK2-CT-1999-00020, PREDICATE) is also gratefully acknowledged. Computations have been done at the Institut du Développement et des Ressources en Informatique Scientifique and at the Centre de Calcul et de Recherche from the University Pierre et Marie Curie.

REFERENCES

Bryan, K., 1984: Accelerating the convergence to equilibrium of ocean–climate models. *J. Phys. Oceanogr.,* **14,** 666–673.

Colin de Verdière, A., 1989: Buoyancy driven planetary flows. *J. Mar. Res.,* **46,** 215–265.

Cox, M. D., 1985: An eddy resolving numerical model of the ventilated thermocline. *J. Phys. Oceanogr.,* **15,** 1312–1324.

Delworth, T., 1996: North Atlantic interannual variability in a coupled ocean–atmosphere model. *J. Climate,* **9,** 2356–2375.

——, S. Manabe, and R. J. Stouffer, 1993: Interdecadal variations of the thermohaline circulation in a coupled ocean–atmosphere model. *J. Climate,* **6,** 1993–2011.

Deser, C., and M. Blackmon, 1993: Surface climate variations over the North Atlantic Ocean during winter: 1900–1989. *J. Climate,* **6,** 1743–1753.

Eden, C., and J. Willebrandt, 2001: Mechanism of interannual to decadal variability of the North Atlantic Circulation. *J. Climate,* **14,** 2266–2280.

Ezer, T., 1999: Decadal variability of the upper layers of the subtropical North Atlantic: An ocean model study. *J. Phys. Oceanogr.,* **29,** 3111–3124.

Grötzner, A., M. Latif, and T. P. Barnett, 1998: A decadal climate cycle in the North Atlantic Ocean as simulated by the ECHO coupled GCM. *J. Climate,* **11,** 831–847.

Häkkinen, S., 1999: Variability of the simulated meridional heat transport in the North Atlantic for the period 1951–1993. *J. Geophys. Res.,* **104,** 10 991–11 007.

——, 2000: Decadal air–sea interaction in the North Atlantic based on observations and modeling results. *J. Climate,* **13,** 1195–1218.

Halliwell, G. R., 1998: Simulation of North Atlantic decadal/multidecadal winter SST anomalies driven by basin-scale atmospheric circulation anomalies. *J. Phys. Oceanogr.,* **28,** 5–21.

Hansen, D. V., and H. Bezdeck, 1996: On the nature of decadal anomalies in North Atlantic sea surface temperature. *J. Geophys. Res.,* **101,** 8749–8758.

Holland, W. R., 1977: Ocean general circulation models. *The Sea.* Vol. 6: *Marine Modeling,* E. D. Golberg et al., Eds., Wiley, 3–45.

Hurrel, J. W., 1995: Decadal trends in the North Atlantic Oscillation: Regional temperature and precipitation. *Science,* **269,** 676–679.

——, and H. Van Loon 1997: Decadal variations in climate associated with the North Atlantic Oscillation. *Climatic Change,* **36,** 301–326.

Kushnir, Y., 1994: Interdecadal variations in North Atlantic sea surface temperature and associated atmospheric conditions. *J. Climate,* **7,** 141–157.

Levitus, S., 1986: Annual cycle of salinity and salt storage in the world ocean. *J. Phys. Oceanogr.,* **16,** 322–343.

Liu, Z., 1999: Forced planetary wave response in a thermocline gyre. *J. Phys. Oceanogr.,* **29,** 1036–1055.

Marshall, J., A. Adcroft. C. Hill, L. Perelman, and C. Heisey, 1997: A finite volume, incompressible Navier Stokes model for studies of the ocean on parallel computers. *J. Geophys. Res.,* **102,** 5753–5766.

——, H. Johnson, and J. Goodman, 2000: A study of the interaction of the North Atlantic Oscillation with ocean circulation. *J. Climate,* **13,** 3711–3719.

McCartney, M. S., R. G. Curry, and H. F. Bezdek, 1997: North Atlantic's transformation pipeline chills and redistributes subtropical water. *Oceanus,* **39** (2), 19–23.

Sirven, J., and C. Frankignoul, 2000: Variability of the thermocline due to the sudden change in the Ekman pumping. *J. Phys. Oceanogr.,* **30,** 1776–1789.

Sturges, W., and B. G. Hong, 1995: Wind forcing of the Atlantic thermocline along 32°N at low frequencies. *J. Phys. Oceanogr.,* **25,** 1706–1715.

——, ——, and A. J. Clarke, 1998: Decadal wind forcing of the North Atlantic subtropical gyre. *J. Phys. Oceanogr.,* **28,** 659–668.

Sutton, R. T., and M. R. Allen, 1997: Decadal predictability of North Atlantic sea surface temperature and climate. *Nature,* **388,** 563–567.

Wallace, J. M., 1996: Observed climatic variability: Spatial structure. *Decadal Climate Variability Dynamics and Predictability,* L. T. Anderson and J. Willebrand, Eds., NATO ASI Series, Vol. 144, Springer Verlag, 30–81.